Available online at www.sciencedirect.com
SCIENCE DIRECT®
Journal of Sound and Vibration 279 (2005) 699–722
JOURNAL OF SOUND AND VIBRATION
www.elsevier.com/locate/jsvi

Free vibrations of multi-girder and multi-cell box bridges with transverse deformations effects

E. Hamed, Y. Frostig*

Department of Structural Engineering, Faculty of Civil and Environmental Engineering, Technion–Israel Institute of Technology, Haifa 32000, Israel

Received 21 July 2003; accepted 13 November 2003

Abstract

A general mathematical approach is developed for the free vibration behaviour analysis of multi-girder and multi-cell box bridges with a single or multi span, including the effects of the transverse deformations of the bridge cross-section. The governing equations of motion and the corresponding boundary and continuity conditions are derived via the variational principle of virtual work following Hamilton's principle. The model is general and valid for any boundary and continuity conditions, and is applicable for multi-girder bridges with longitudinal and cross beams and for multi-cell box bridges. The warping and the distortion of the bridge cross-section effects are included in the proposed model. Closed-form solutions of the governing equations are derived and the Newton–Raphson method is used to determine the eigenfrequencies. Numerical examples are presented to validate the proposed model, and are also used to examine the accuracy of other approximate models used in the analysis of bridges. The results of the proposed model are validated through comparison with three-dimensional finite element models. The results reveal that the transverse deformations decrease the magnitudes of the eigenfrequencies of the torsional mode shapes, as well as the high flexural modes.

1. Introduction

Loaded multi-girder and multi-cell box bridges undergo several deformation shapes, such as flexural and torsional deformations (see Figs. 1a and b). In both types of bridges, they undergo transverse deformations and distortion of the cross-section (see Fig. 1c). The transverse

*Corresponding author. Tel.: +97-248293046; fax: +97-248295697.
E-mail address: cvrfros@techunix.technion.ac.il (Y. Frostig).

0022-460X/$ - see front matter © 2003 Elsevier Ltd. All rights reserved.
doi:10.1016/j.jsv.2003.11.037

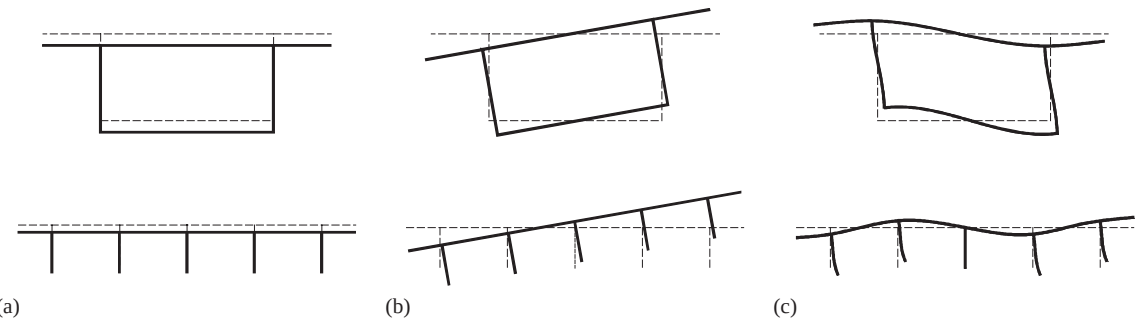

Fig. 1. Deformation components in bridges: (a) flexure; (b) torsion; (c) distortion and transverse deformations.

deformations and distortion of the cross-section are of great interest mainly in the analysis of thin-walled bridges. The distortion of the cross-section yields a redistribution of the normal and shear stresses in the longitudinal direction, and in many cases should be considered. Most important is the effect of the transverse inertial forces and bending moments in the free vibration analysis of bridges. These inertial forces may significantly affect the magnitudes of the eigenfrequencies of bridges. Hence, ignoring these inertial forces may lead to an erroneous eigenfrequencies of the torsional eigenmodes in particular. Although, a wide range of analytical and numerical methods are available for the dynamic and free vibration analyses of bridges, many of them do not consider the transverse deformations effects at all, and others consider them based on some approximate assumptions. Furthermore, these methods suffer from severe limitations and applicability. A literature survey is provided ahead, and it includes only papers that deal with the dynamic analysis of bridges.

In general, many research works deal with the dynamic analysis of multi-cell box and multi-girder bridges. However, there are only very few approaches these research works can be categorized in. The first one models the bridge as a classical beam, which uses Bernoulli–Euler assumptions [1,2]. In this model only vertical deflections and rigid-body rotations are considered. Hence, some eigenmodes that are controlled by the torsional warping and distortion of the bridge cross-section cannot be detected by this approach. These eigenmodes yield low frequencies that affect the dynamic behaviour of bridges. Following the same approach, some research works [3–5] have introduced the torsional warping effects into the differential equations of motion. A fundamental contribution to the general solution of this problem was given by Vlasov [6] and followed by Dabrowski [7]. Timoshenko et al. [8] have presented an analytical solution to the equations of motion that include the torsional warping effects. However, this method ignores the transverse inertial forces and the effects of the cross-section distortion. Again, these inertial forces may lead to a significant reduction in the eigenfrequencies of the torsional eigenmodes particularly.

The third approach is based on a finite strip idealization of the bridge deck [9,10]. In this model, it is assumed that the longitudinal behaviour of each strip is a linear combination of the eigenmodes of a beam with the same boundary conditions as the strip. Here, the transverse deformations and inertial forces are considered using a cubic interpolation function in the transverse direction. The main deficiency of this model is the assumption that the cubic

polynomial is accurate for all eigenmodes, which contradicts reality. Hence, a large number of strips is required to reach a reliable solution. Moreover, the implementation of this approach for continuous bridges is problematic.

The orthotropic plate approach for the free vibration analysis of bridges [11] is an approximate one, owing to the assumption of uniform distribution of the mass and the flexural and torsional rigidities through the width and the length of the bridge. This assumption might be far from the real one, especially in box bridges, and leads to erroneous results. Furthermore, the application of this approach for continuous bridges and general boundary conditions is complicated. The fifth approach is the planar grillage beam (GRID) [12–14]. This approach ignores the out of plane or the transverse deformations of the longitudinal beams, as well as the flexibility of the equivalent flanges of the longitudinal beams in the transverse direction. These deficiencies affect the predicted values of the eigenfrequencies of the bridge.

Huang et al. [15] presented a procedure for obtaining the dynamic response of thin-walled box bridges. The box girder was divided into a number of thin-walled beam elements in the longitudinal direction, which include the warping and distortion of the cross-section in an approximate form. The distortion of the cross-section is described by an additional degree of freedom, which is the distortional angle of the cross-section (see Ref. [16]). This approach considers only the effects of the distortion of the cross-section on the longitudinal normal and shear stresses, while the effects of the associated transverse inertial forces involved with the distortion action are not considered in this approach.

The last approach is the finite element model. In most cases, a three-dimensional finite element model may offer a comprehensive treatment with the free vibration analysis of bridges [17,18]. The transverse deformations in this model are considered by using shell elements for modelling the slab and the longitudinal girders. The FE model is a general numerical tool that is complicated for use when parametric studies are of concern.

The literature survey reveals that the aforementioned traditional methods commonly used for the static and dynamic analysis of bridges, are inaccurate for the free vibration analysis of bridges in general, and for thin-walled box bridges in particular. The deficiency of these models is due to their approximate treatment of the effects of the transverse inertial forces, and due to their severe limitations and applicability. In this study, a general mathematical approach for the free vibration analysis of multi-girder and multi-cell box bridges that is based on a variational approach is developed, and it considers the transverse inertial forces in an accurate form. The variational principle of virtual work is used to derive the field and governing equations of motion, and their associated boundary and continuity conditions. The model fulfills any kind of boundary and continuity conditions and is applicable for multi-girder bridges with cross beams, for multi-cell box bridges, and for composite construction of bridges. In the analysis, the bridge is modelled as made of plates or panels that are interconnected through equilibrium and compatibility in the longitudinal and transverse directions. Each panel undergoes four kinds of deformations: longitudinal, in-plane deflection, out-of-plane deflection and a Saint-Venant type of torsion. Hence, each panel behaves as a unidirectional plate in the transverse direction and as a classical beam that follows the Bernoulli–Euler assumptions in the longitudinal direction. It is important to indicate that the slab is divided into a number of sub-slabs in the transverse analysis, where each sub-slab is bounded by two longitudinal beams or by one beam and the free edge of the

slab. While in the longitudinal analysis, it is assumed that the slab behaves as a single beam that follows the Bernoulli–Euler assumptions. This modelling of bridges enables the warping and the distortion of the bridge cross-section to be included in an accurate form. It is assumed that the deformations are small. In addition, since most bridges are composed of precast concrete girders, it is assumed that the cross beams in multi-girder bridges are able to transfer only shear forces between the longitudinal beams. The effects of the longitudinal vibrations and the rotary inertia have been neglected.

The mathematical formulation is presented ahead, and it includes the equations of motion for a general multi-girder and multi-cell box bridge, as well as the associated boundary and continuity conditions. The mathematical formulation is followed by some numerical examples that include: (1) comparison between the results of the proposed model and those of other models that appear in the literature survey; (2) numerical study of the effect of transverse deformations on the magnitudes of the eigenfrequencies; (3) validation of the proposed model results through comparison with three-dimensional finite element results. Summary and conclusions appear in the sequel.

2. Mathematical formulation

The variational calculus of virtual work is used to formulate only two models for two types of bridges for the sake of brevity and simplicity, although it is possible to formulate a general model for bridges with a general cross-section. The first model deals with the free vibration behaviour of multi-girder bridges, which include cross beams through the length of the bridge, and the second one discusses the free vibration behaviour of general multi-cell box bridges. The mathematical formulation includes the derivation of the field and governing equations of motion, along with the boundary and continuity conditions.

2.1. Multi-girder bridges

The geometry, and sign convention of the co-ordinates and the deformations of a multi-girder bridge appear in Fig. 2, where y and z are local co-ordinates for each panel, and measured downwards from the centroid of each panel in the transverse and longitudinal directions, x is a global longitudinal co-ordinate. Notice that Fig. 2 describes a specific case of a continuous bridge with four longitudinal beams and one cross beam. However, the mathematical formulation is general, and the equations of motion and the boundary/continuity conditions are valid for any type of multi-girder bridges with a general layout.

The equations of motion and the boundary/continuity conditions are rigorously derived via the variational principle of energy minimization following Hamilton's principle, which requires:

$$\delta \int_{t_1}^{t_2} (T - U)\,\mathrm{d}t = 0, \tag{1}$$

where T is the kinetic energy, U is the internal potential energy, δ is the variational operator and t is the time co-ordinate.

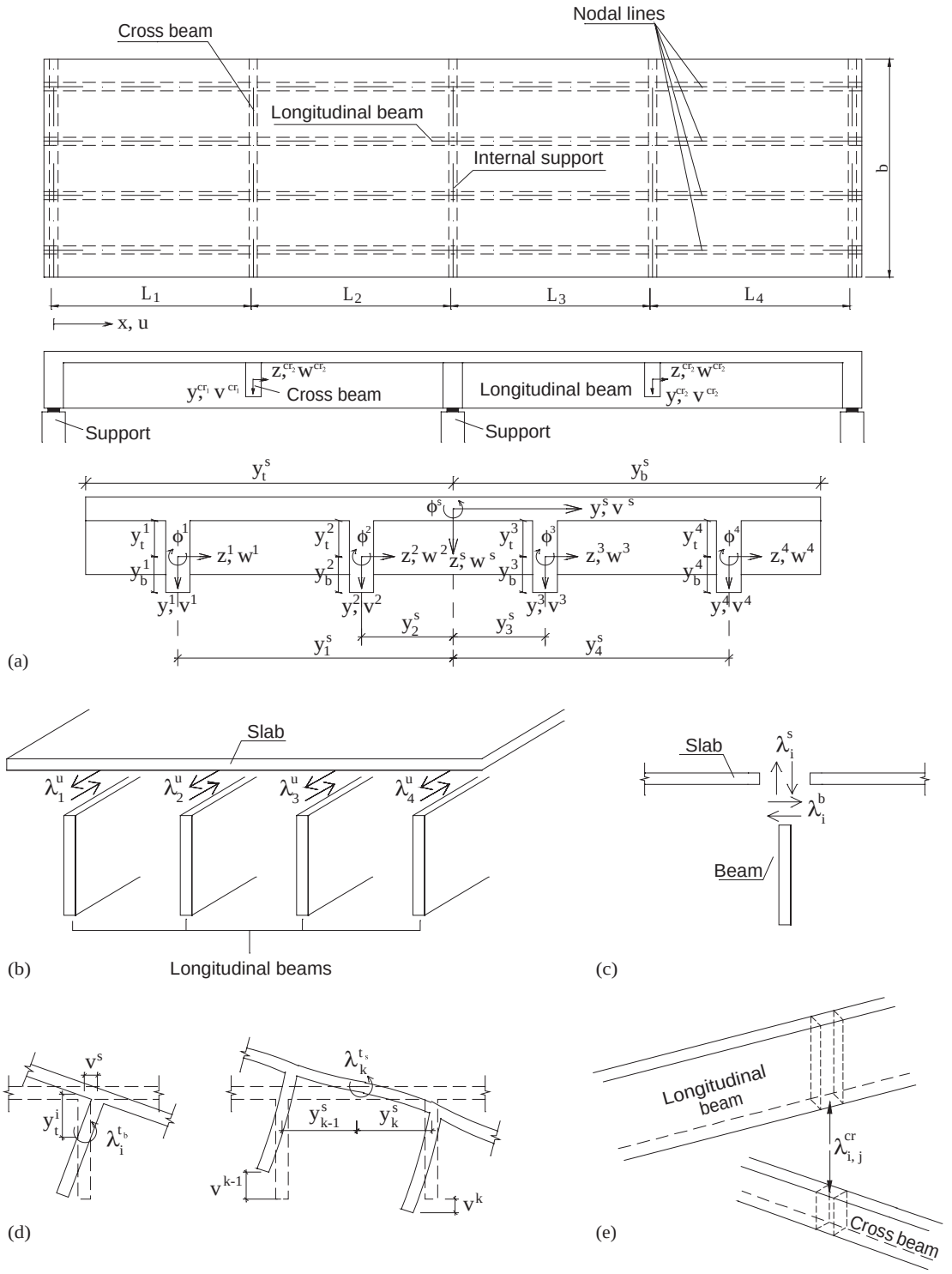

Fig. 2. A typical multi-girder bridge: (a) sign convention; (b) longitudinal shear flow along the nodal lines; (c) transverse shear forces at the nodal lines; (d) torsional moments due to in-plane deflections; (e) shear forces between the longitudinal girders and the transverse ones.

The first variation of the kinetic energy, which includes in-plane and out-of-plane inertial forces, as well as rotary inertia due to local torsion of the panels equals

$$\begin{aligned}\delta T = &\int_x m_x^s \dot{v}^s \delta\dot{v}^s \,\mathrm{d}x + \int_x \int_y m_y^s \dot{w}^s \delta\dot{w}^s \,\mathrm{d}y\,\mathrm{d}x + \int_x \rho^s I_p^s \dot{\phi}^s \delta\dot{\phi}^s \,\mathrm{d}x \\ &+ \sum_{i=1}^{n_b}\left[\int_x m_x^i \dot{v}^i \delta\dot{v}^i \,\mathrm{d}x + \int_x \int_y m_y^i \dot{w}^i \delta\dot{w}^i \,\mathrm{d}y\,\mathrm{d}x + \int_x \rho^i I_p^i \dot{\phi}^i \delta\dot{\phi}^i \,\mathrm{d}x\right] \\ &+ \sum_{j=1}^{n_{cr}} \int_y m_y^{cr_j} \dot{v}^{cr_j} \delta\dot{v}^{cr_j} \,\mathrm{d}y, \end{aligned} \tag{2}$$

where the superscript s denotes all quantities related to the slab, the superscript $i = 1, 2, \ldots, n_b$ denotes all quantities related to each longitudinal beam, where n_b is the number of the longitudinal beams, the superscript cr_j $(j = 1, 2, \ldots, n_{cr})$ denotes all quantities related to each cross beam, where n_{cr} is the number of the cross beams, m_j $(j = x, y)$ is the mass per unit length in the x and y direction, ρ is the mass density, I_p is the polar moment of inertia and $(\cdot)$ denotes a derivative with respect to time.

The first variation of the potential energy equals

$$\begin{aligned}\delta U = &\int_{V^s} \sigma_{xx}^s \delta\varepsilon_{xx}^s \,\mathrm{d}V + \int_{V^s} \tau_{xy}^s \delta\gamma_{xy}^s \,\mathrm{d}V + \int_{V^s} \tau_{xz}^s \delta\gamma_{xz}^s \,\mathrm{d}V + \sum_{k=1}^{n_s} \int_{V^{s_k}} \sigma_{yy}^{s_k} \delta\varepsilon_{yy}^{s_k} \,\mathrm{d}V^{s_k} \\ &+ \sum_{i=1}^{n_b}\left[\int_{V^i} \sigma_{xx}^i \delta\varepsilon_{xx}^i \,\mathrm{d}V + \int_{V^i} \tau_{xy}^i \delta\gamma_{xy}^i \,\mathrm{d}V + \int_{V^i} \tau_{xz}^i \delta\gamma_{xz}^i \,\mathrm{d}V + \int_{V^i} \sigma_{yy}^i \delta\varepsilon_{yy}^i \,\mathrm{d}V\right] \\ &+ \sum_{j=1}^{n_{cr}} \int_{V^{cr_j}} \sigma_{yy}^{cr_j} \delta\varepsilon_{yy}^{cr_j} \,\mathrm{d}V + \int_x \sum_{i=1}^{n_b} \delta[\lambda_i^u (u^i(y_t^i) - u^s(y_i^s))] \,\mathrm{d}x \\ &+ \int_x \sum_{k=1}^{n_s} \delta\left[\lambda_k^{t_s}\left(\phi^{s_k} - \frac{v^{k-1} - v^k}{y_{k-1}^s - y_k^s}\right)\right] \mathrm{d}x + \int_x \sum_{i=1}^{n_b} \delta\left[\lambda_i^{t_b}\left(\phi^i - \frac{v^s}{y_t^i}\right)\right] \mathrm{d}x \\ &+ \int_x \sum_{i=1}^{n_b} \delta[\lambda_i^b (w^i(y_t^i) + v^s)] \,\mathrm{d}x + \int_x \sum_{i=1}^{n_b} \delta[\lambda_i^s (w^s(y_i^s) - v^i)] \,\mathrm{d}x \\ &+ \sum_{j=1}^{n_{cr}} \sum_{i=1}^{n_b} \delta[\lambda_{i,j}^{cr} (v^i(L_j) - v^{cr_j}(y_i^s))], \end{aligned} \tag{3}$$

where ε_{ii} and σ_{ii} $(i = x, y)$ are the longitudinal and transverse strains and normal stresses, respectively, in each panel, γ_{xi} and τ_{xi} $(i = y, z)$ are the shear strains and stresses, respectively, due to longitudinal torsion of each panel relative to its centroid, u is the longitudinal deformation of each panel along the nodal lines, w is the out-of-plane deflection, v is the in-plane deflection, ϕ is the torsional angle, V is the volume of each panel, λ are Lagrange multipliers that impose identical deformations and fulfill the compatibility conditions between the various constituents of the structure (see Fig. 2 and a detailed description next), ε_{yy}^{cr} and σ_{yy}^{cr} are the strain and normal stress through the length of each cross beam, v^{cr} is the vertical deflection of each cross beam. In order to fulfill the compatibility requirements between

the constituents of the structure, the slab is divided into n_s sub-slabs in the transverse analysis, while each sub-slab is bounded by two longitudinal beams or by one beam and the free edge of the slab, and is denoted by the superscript s_k $(k = 1, 2, \ldots, n_s)$. Similarly, each cross beam is divided into n_s beams. It is important to indicate that the transverse axial deformations in the local y direction of each panel are neglected.

The kinematic and constitutive relations for each panel in the transverse and longitudinal directions using Hooke's law, are

$$\varepsilon_{yy} = -zw_{,yy}\,, \qquad \varepsilon_{xx} = u_{o,x} - yv_{,xx}\,, \tag{4, 5}$$

$$\gamma_{xy} = -z\phi_{,x}\,, \quad \gamma_{xz} = y\phi_{,x}\,, \tag{6}$$

$$\sigma_{xx} = E\varepsilon_{xx}, \quad \sigma_{yy} = E\varepsilon_{yy}, \tag{7}$$

$$\tau_{xy} = G\gamma_{xy}, \quad \tau_{xz} = G\gamma_{xz}, \tag{8}$$

where E is the modulus of elasticity, G is the shear modulus, u_o is the longitudinal deformation at the centroid of each panel, $(\,)_{,x}$ and $(\,)_{,y}$ denote differentiation with respect to x and y, respectively.

The kinematic and constitutive relations for each cross beam are

$$\varepsilon^{cr}_{yy} = -yv^{,cr}_{,yy}\,, \quad \sigma^{cr}_{yy} = E^{cr}\varepsilon^{cr}_{yy}, \tag{9}$$

where E^{cr} is the modulus of elasticity of each cross beam. It is assumed that the cross beams are capable to transfer only shear forces between the longitudinal beams (see Fig. 2e).

The variational formulation is applied for each panel separately, along with the use of Lagrange multipliers that constrain compatibility conditions between the various constituents of the structure. Four necessary compatibility conditions that interconnect the panels are considered.

1. *Longitudinal deformations compatibility between the longitudinal beams and the slab, through the nodal lines*. Thus

$$u^i(y = y^i_t) = u^s(y = y^s_i), \tag{10}$$

where $u^i(y = y^i_t)$ is the longitudinal deformation of the ith longitudinal beam at its upper interface (see Eq. (11) ahead), y^i_t is the vertical co-ordinate of the upper interface of the ith longitudinal beam measured downwards from its centroid (see Fig. 2a), $u^s(y = y^s_i)$ is the longitudinal deformation of the slab at the ith nodal line (see Eq. (11)) and y^s_i is the horizontal co-ordinate of the ith nodal line measured rightwards from the centroid of the slab (see Fig. 2a). Thus

$$u^i(y = y^i_t) = u^i_{ox} - y^i_t v^{,i}_{,x}\,, \quad u^s(y = y^s_i) = u^s_{ox} - y^s_i v^{,s}_{,x}\,. \tag{11}$$

These compatibility conditions are fulfilled through the introduction of Lagrange multipliers $\lambda^u_i(x)$, $(i = 1, \ldots, n_b)$ into the potential energy of the structure (see Eq. (3)). Actually, each Lagrange multiplier represents the longitudinal shear flow between the ith beam and the slab along the ith nodal line (see Fig. 2b).

2. *Rotation compatibility between the slab and the longitudinal beams*. It is assumed that the torsion of each sub-slab and longitudinal beam depends on the in-plane deflections of the constituents of the structure only. Thus, the torsional angle of each sub-slab is determined by the differential vertical deflections of its bounded beams (Eq. (12)), and the torsional angle of

each beam is determined by the in-plane deflection of the slab (Eq. (13)), and they read

$$\phi^{s_k} = \frac{(v^{k-1} - v^k)}{(y^s_{k-1} - y^s_k)}, \qquad \phi^i = \frac{v^s}{y^i_t}. \tag{12, 13}$$

These compatibility conditions are considered through the use of Lagrange multipliers $\lambda_i^{t_s}(x)$ and $\lambda_i^{t_b}(x)$, see Eq. (3), which are distributed torsional moments through the length of the bridge (see Fig. 2d).

3. *Transverse compatibility at the nodal lines in z and y directions*. The horizontal deflection of each longitudinal beam at its interface with the slab must equal the horizontal deflection of the slab, and in addition the vertical deflection of each longitudinal beam must be identical to that of slab at the nodal line. Hence, these compatibility conditions read

$$w^i(y = y^i_t) = -v^s, \qquad w^s(y = y^s_i) = v^i. \tag{14, 15}$$

These conditions are imposed by Lagrange multipliers $\lambda_i^b(x)$ and $\lambda_i^s(x)$ (see Eq. (3)), where $\lambda_i^b(x)$ is the out-of-plane shear force in the ith longitudinal beam at the ith nodal line (see Fig. 2c), and $\lambda_i^s(x)$ is the out-of-plane shear force in the slab at the ith nodal line (see Fig. 2c).

4. *Vertical deflections compatibility between the longitudinal beams and the cross ones at the connection location*. Thus

$$v^i(x = L_j) = v^{cr}(y = y^s_i). \tag{16}$$

Discrete Lagrange multipliers $\lambda^{cr}_{i,j}$, $(i = 1, \ldots, n_b; j = 1, \ldots, n_{cr})$ are introduced (see Eq. (3)) in order to impose this condition (see Fig. 2e).

The governing equations of motion, as well as the boundary and continuity conditions are derived using Eqs. (1)–(3), along with the use of the kinematic and constitutive relations (4)–(9). Hence, after some algebraic manipulations and integration by parts, the governing equations of motion in the transverse direction of each sub-slab and longitudinal beam read

$$m^s_y \ddot{w}^s - M^s_{yy,yy} = 0, \qquad \rho I^s_p \ddot{\phi}^s - M^s_{t,x} + \lambda^{t_s}_i = 0, \tag{17, 18}$$

$$m^i_y \ddot{w}^i - M^i_{yy,yy} = 0, \qquad \rho I^i_p \ddot{\phi}^i - M^i_{t,x} + \lambda^{t_b}_i = 0, \tag{19, 20}$$

where M^m_t and M^m_{yy}, $(m = s, i)$ are the torsional and transverse bending moments, respectively, in each sub-slab and longitudinal beam.

The governing equations of motion in the longitudinal direction are as follows:

$$-N^s_{xx,x} - \sum_{i=1}^{n_b} \lambda^u_i = 0, \tag{21}$$

$$m^s_x \ddot{v}^s - M^s_{xx,xx} + \sum_{i=1}^{n_b} [-\lambda^u_{i,x} y^s_i - \lambda^{t_b}_i / y^i_t + \lambda^b_i] = 0, \tag{22}$$

$$-N^i_{xx,x} + \lambda^u_i = 0, \tag{23}$$

$$m^i_x \ddot{v}^i - M^i_{xx,xx} + \lambda^u_{i,x} y^i_t - \frac{\lambda^{t_s}_{i+1}}{(y^s_i - y^s_{i+1})} + \frac{\lambda^{t_s}_i}{(y^s_{i-1} - y^s_i)} - \lambda^s_i = 0, \tag{24}$$

where N_{xx}^k and M_{xx}^k, $(k = s, i)$ are the stress resultants and the bending moments in the longitudinal direction of the slab and each longitudinal beam, respectively.

The equation of motion of each cross beam equals

$$m_y^{cr}\ddot{v}^{cr} - M_{yy,yy}^{cr} = 0, \tag{25}$$

where M_{yy}^{cr} is the bending moment of each cross beam.

The boundary and continuity conditions are as follows:

At the edges of the slab ($y = y_b^s$ and $y = y_t^s$, see Fig. 2a) they read

$$M_{yy}^s = 0 \quad \text{or} \quad w,_y^s = 0, \tag{26}$$

$$M_{yy,y}^s = 0 \quad \text{or} \quad w_y^s = 0. \tag{27}$$

At the bottom of each longitudinal beam ($y = y_b^i$, see Fig. 2a) they read

$$M_{yy}^i = 0 \quad \text{or} \quad w,_y^i = 0, \tag{28}$$

$$M_{yy,y}^i = 0 \quad \text{or} \quad w_y^i = 0. \tag{29}$$

At each nodal line they read

$$M_{yy}^{s_i}(y_i^s) - M_{yy}^i(y_t^i) + M_{yy}^{s_{i+1}}(y_i^s) = 0, \tag{30}$$

$$w,_y^{s_i}(y_i^s) - w,_y^{s_{i+1}}(y_i^s) = 0, \tag{31}$$

$$w,_y^i(y_t^i) + w,_y^{s_i}(y_i^s) = 0, \qquad w_y^{s_i}(y_i^s) - w_y^{s_{i+1}}(y_i^s) = 0, \tag{32, 33}$$

$$w^{s_i}(y_i^s) = v^i, \qquad w^i(y_t^i) = -v^s, \tag{34, 35}$$

$$-M_{yy,y}^{s_i}(y_i^s) + \lambda_i^s + M_{yy,y}^{s_{i+1}}(y_i^s) = 0, \tag{36}$$

$$-M_{yy,y}^i(y_t^i) + \lambda_i^b = 0. \tag{37}$$

The boundary conditions in the longitudinal direction at $x = 0$ and L, read

$$N_{xx}^s + \sum_{i=1}^{n_b} N_{xx}^i = 0 \quad \text{or} \quad u_o^s = 0, \tag{38}$$

$$M_{xx}^s + \sum_{i=1}^{n_b} N_{xx}^i y_i^s = 0 \quad \text{or} \quad v,_x^s = 0, \tag{39}$$

$$M_{xx,x}^s + \sum_{i=1}^{n_b} [\lambda_i^u y_i^s + M_t^i / y_t^i] = 0 \quad \text{or} \quad v^s = 0, \tag{40}$$

$$-M_{xx}^i + N_{xx}^i y_t^i = 0 \quad \text{or} \quad v,_x^i = 0, \tag{41}$$

$$M_{xx,x}^i - \lambda_i^u y_t^i - M_t^{s_i}/(y_{i-1}^s - y_i^s) + M_t^{s_{i+1}}/(y_i^s - y_{i+1}^s) = 0 \quad \text{or} \quad v^i = 0. \tag{42}$$

The continuity conditions at $x = L_j$, where a typical cross beam is located, are

$$N_{xx}^{s,left} + \sum_{i=1}^{n_b} N_{xx}^{i,left} = N_{xx}^{s,right} + \sum_{i=1}^{n_b} N_{xx}^{i,right}, \tag{43}$$

$$-M_{xx}^{s,left} - \sum_{i=1}^{n_b} N_{xx}^{i,left} y_i^s = -M_{xx}^{s,right} - \sum_{i=1}^{n_b} N_{xx}^{i,right} y_i^s, \tag{44}$$

$$v,_x^{s,left} = v,_x^{s,right}, \tag{45}$$

$$M_{xx,x}^{s,left} + \sum_{i=1}^{n_b} [\lambda_i^{u,left} y_i^s + M_t^{i,left}/y_t^i] = M_{xx,x}^{s,right} + \sum_{i=1}^{n_b} [\lambda_i^{u,right} y_i^s + M_t^{i,right}/y_t^i], \tag{46}$$

$$v^{s,left} = v^{s,right}, \tag{47}$$

$$-M_{xx}^{i,left} + N_{xx}^{i,left} y_t^i = -M_{xx}^{i,right} + N_{xx}^{i,right} y_t^i, \tag{48}$$

$$v,_x^{i,left} = v,_x^{i,right}, \tag{49}$$

$$\begin{aligned} M_{xx,x}^{i,left} - \lambda_i^{u,left} y_t^i - M_t^{s_i,left}/(y_{i-1}^s - y_i^s) + M_t^{s_{i+1},left}/(y_i^s - y_{i+1}^s) + \lambda_{i,j}^{cr} \\ = M_{xx,x}^{i,right} - \lambda_i^{u,right} y_t^i - M_t^{s_i,right}/(y_{r_{i-1}}^s - y_{r_i}^s) + M_t^{s_{i+1},right}/(y_i^s - y_{i+1}^s). \end{aligned} \tag{50}$$

The boundary conditions at $y = y_b^s$ and $y = y_t^s$ of each cross beam are

$$M_{yy}^{cr} = 0 \quad \text{or} \quad v,_y^{cr} = 0, \tag{51}$$

$$M_{yy,y}^{cr} = 0 \quad \text{or} \quad v^{cr} = 0. \tag{52}$$

The continuity conditions of each field in every cross beam, read

$$M_{yy}^{cr_i} = M_{yy}^{cr_{i+1}}, \qquad v,_y^{cr_i} = v,_y^{cr_{i+1}}, \tag{53, 54}$$

$$v^{cr_i} = v^{cr_{i+1}}, \qquad v^{cr_i} = v^i, \tag{55, 56}$$

$$-M_{yy,y}^{cr_i} + \lambda_{i,j}^{cr} + M_{yy,y}^{cr_{i+1}} = 0. \tag{57}$$

The free vibration problem is solved for harmonic behaviour in time of $\exp(i\omega t)$, where i is the imaginary unit and ω is the eigenfrequency. Thus the governing equations of motion of the free

vibration are replaced by algebraic and linear differential equations that are solved analytically in a closed form. The eigenfrequencies and the eigenmodes are determined through the use of Newton–Raphson method.

2.2. Multi-cell box bridges

The equations of motion and the boundary/continuity conditions of a general multi-cell box bridge without internal diaphragms are derived via the variational principle of virtual work, following the procedure described in the previous section, with the neglect of the local torsional rigidity of each panel along the bridge. The geometry, and sign convention of the co-ordinates and the deformations appear in Fig. 3. The kinematic and constitutive relations used here, are the same as in the previous chapter.

The compatibility conditions required here are as follows:

1. *Longitudinal deformations compatibility between the various structure constituents through the nodal lines.*

$$u^i(y = y_t^i) = u^{us}(y = y_i^{us}), \tag{58}$$

$$u^i(y = y_b^i) = u^{ls}(y = y_i^{ls}), \tag{59}$$

where

$$u^i(y = y_t^i) = u_{ox}^i - y_t^i v_{,x}^i, \qquad u^{us}(y = y_i^{us}) = u_{ox}^{us} - y_i^{us} v_{,x}^{us}, \tag{60,61}$$

$$u^i(y = y_b^i) = u_{ox}^i - y_b^i v_{,x}^i, \qquad u^{ls}(y = y_i^{ls}) = u_{ox}^{ls} - y_i^{ls} v_{,x}^{ls}, \tag{62,63}$$

the superscript *us* denotes all quantities related to the upper slab, the superscript *ls* denotes all quantities related to the lower slab, the superscript $i = 1, 2, \ldots, n_p$ denotes all quantities related to each side panel, while n_p is the number of the side panels, y_i^{us} and y_i^{ls} are the horizontal co-ordinates of the upper and lower interfaces of the ith side panel, measured rightward from the centre of the upper and lower slabs respectively, see Fig. 3a. These compatibility conditions are introduced by the use of Lagrange multipliers $\lambda_i^{u,us}(x)$ and $\lambda_i^{u,ls}(x)$, which describe the shear flow between the slabs and the ith side panel along the nodal lines, see Fig. 3b.

2. *Transverse compatibility at the nodal lines in z and y directions.* A relation between the out-of-plane deflections and the in-plane deflections of the panels at the nodal lines is describes herein. For this purpose, consider a general case of two inclined panels (see Fig. 4a). The out-of-plane deflections of the two panels at the nodal lines ($w_{i,i}$ and $w_{i,i-1}$) involved due to in-plane displacements v_i are illustrated in Fig. 4b, and equal to

$$w_{i,i-1} = -\frac{v_i}{\sin(\beta_{i-1} - \beta_i)}, \quad w_{i,i} = -\frac{v_i}{\tan(\beta_{i-1} - \beta_i)}. \tag{64}$$

While those involved due to in-plane displacements v_{i-1} are described in Fig. 4c, and equal to

$$w_{i,i-1} = \frac{v_{i-1}}{\tan(\beta_{i-1} - \beta_i)}, \quad w_{i,i} = \frac{v_{i-1}}{\sin(\beta_{i-1} - \beta_i)}. \tag{65}$$

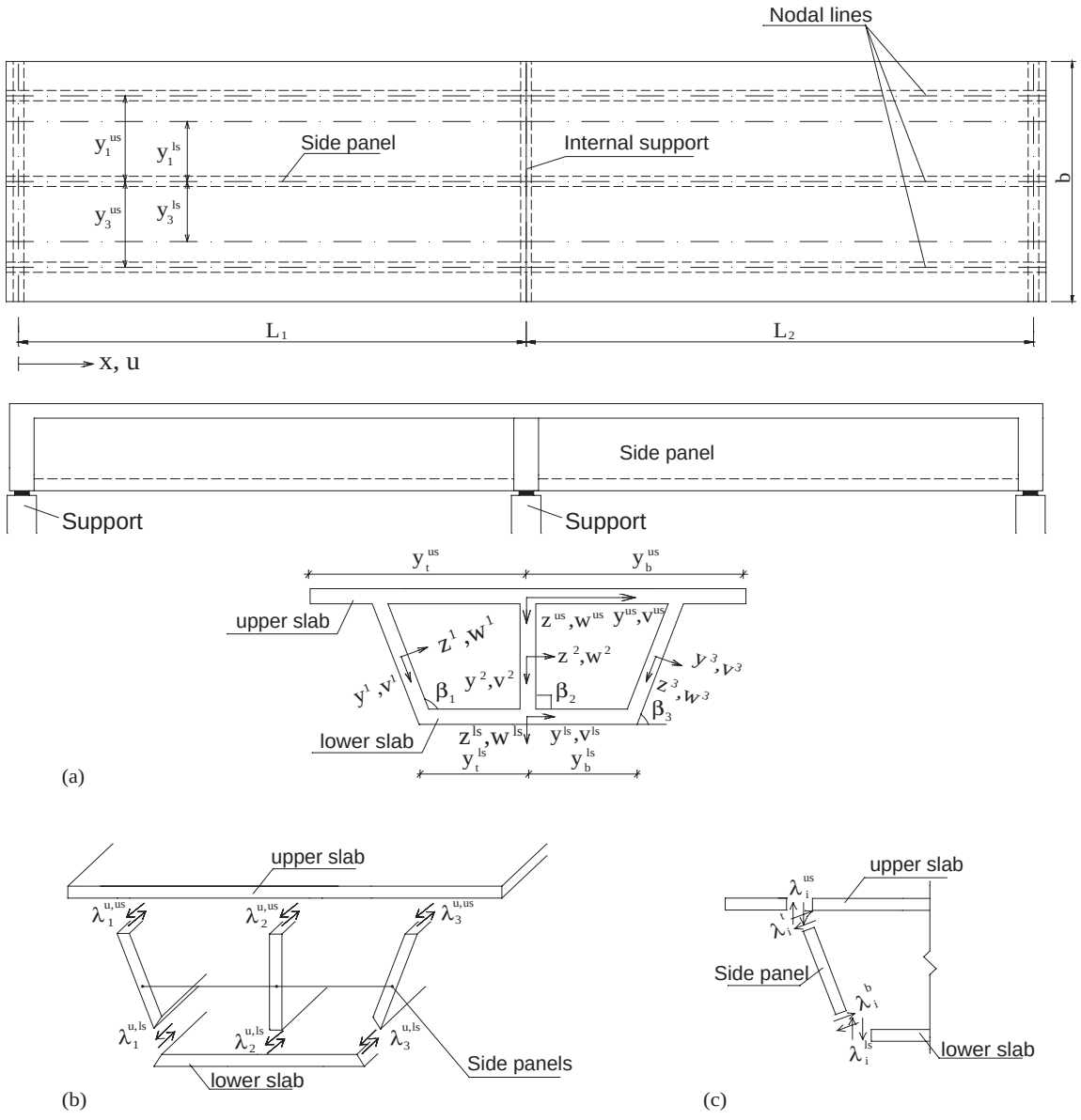

Fig. 3. A typical multi-cell box bridge: (a) sign convention; (b) longitudinal shear flow along the nodal lines; (c) transverse shear forces at the nodal lines.

In the case of a multi-cell box bridge (see Fig. 3), the following compatibility conditions exist at each nodal line:

$$w^i(y = y_t^i) = -\frac{v^{us}}{\sin(\beta_i)} + \frac{v^i}{\tan(\beta_i)}, \tag{66}$$

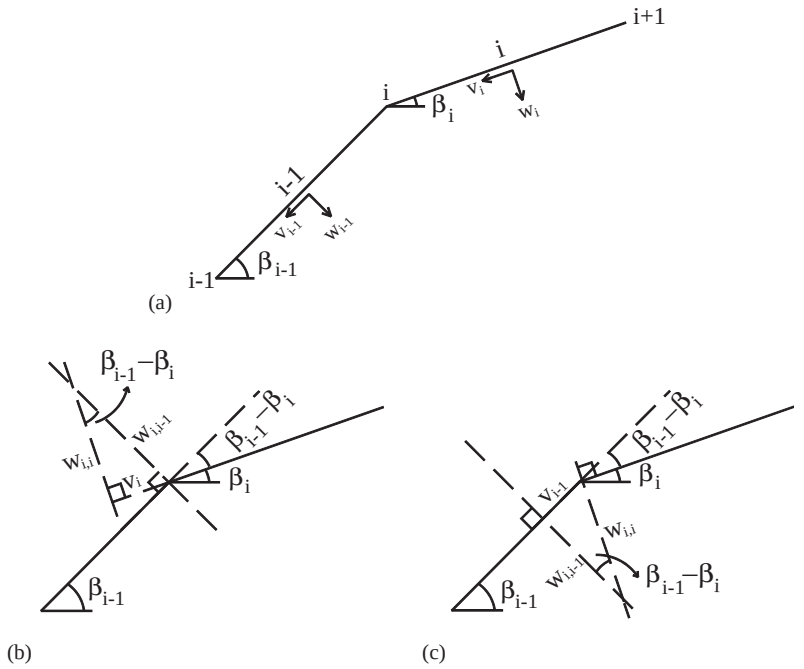

Fig. 4. Geometric relations between the local transverse deflections and the in-plane deflections along the nodal lines. (a) a general case of two inclined panels; (b) v_i displacement; (c) v_{i-1} displacement.

$$w^i(y = y_b^i) = \frac{v^i}{\tan(\beta_i)} - \frac{v^{ls}}{\sin(\beta_i)}, \tag{67}$$

$$w^j(y = y_i^j) = -\frac{v^j}{\tan(\beta_i)} + \frac{v^i}{\sin(\beta_i)}, \tag{68}$$

where $(j = us, ls)$. These compatibility conditions are imposed by Lagrange multipliers $\lambda_i^t(x), \lambda_i^b(x), \lambda_i^{us}(x), \lambda_i^{ls}(x)$. Actually, the Lagrange multipliers are the shear forces of the panels and the slabs at each nodal line, due to transverse bending see Fig. 3c.

For brevity, the first variations of the kinetic and potential energies are not presented. The equations of motion that govern the transverse behaviour of each side panel and sub-slab are

$$m_y^j \ddot{w}^j - M_{yy,yy}^j = 0, \quad j = us, ls, i. \tag{69}$$

The upper and lower slabs are divided into n_{us} and n_{ls} sub-slabs, respectively, in the transverse behaviour analysis; where us_k $(k = 1, 2, \ldots, n_{us})$ designates each upper sub-slab, and ls_k $(k = 1, 2, \ldots, n_{ls})$ designates each lower sub-slab.

The equations of motion in the longitudinal direction of the upper and lower slabs, as well as of each side panel, are as follows:

$$-N_{xx,x}^i + \lambda_i^{u,us} + \lambda_i^{u,ls} = 0, \tag{70}$$

$$m_x^i \ddot{v}^i - M^i_{xx,xx} + \lambda^{u,us}_{i,x} y^i_t + \lambda^{u,ls}_{i,x} y^i_b - \frac{\lambda^t_i}{\tan(\beta_i)} - \frac{\lambda^{us}_i}{\sin(\beta_i)} - \frac{\lambda^b_i}{\tan(\beta_i)} - \frac{\lambda^{ls}_i}{\sin(\beta_i)} = 0, \tag{71}$$

$$-N^{us}_{xx,x} - \sum_{i=1}^{n_p} \lambda^{u,us}_i = 0, \tag{72}$$

$$m_x^{us} \ddot{v}^{us} - M^{us}_{xx,xx} + \sum_{i=1}^{n_b} [-\lambda^{u,us}_{i,x} y^{us}_i + \lambda^t_i/\sin(\beta_i) + \lambda^{us}_i/\tan(\beta_i)] = 0, \tag{73}$$

$$-N^{ls}_{xx,x} - \sum_{i=1}^{n_p} \lambda^{u,ls}_i = 0, \tag{74}$$

$$m_x^{ls} \ddot{v}^{ls} - M^{ls}_{xx,xx} + \sum_{i=1}^{n_p} [-\lambda^{u,ls}_{i,x} y^{ls}_i + \lambda^b_i/\sin(\beta_i) + \lambda^{ls}_i/\tan(\beta_i)] = 0. \tag{75}$$

The transverse boundary conditions of the upper slab at $y = y^{us}_t$ and y^{us}_b, see Fig. 3a, are

$$M^{us}_{yy} = 0 \quad \text{or} \quad w^{us}_{,y} = 0, \tag{76}$$

$$M^{us}_{yy,y} = 0 \quad \text{or} \quad w^{us} = 0. \tag{77}$$

The transverse continuity conditions along the upper nodal lines are

$$M^{us_i}_{yy}(y^{us}_i) - M^i_{yy}(y^i_t) + M^{us_{i+1}}_{yy}(y^{us}_i) = 0, \tag{78}$$

$$w^{us_i}_{,y}(y^{us}_i) - w^{us_{i+1}}_{,y}(y^{us}_i) = 0, \tag{79}$$

$$w^{i}_{,y}(y^i_t) + w^{us_i}_{,y}(y^{us}_i) = 0, \tag{80}$$

$$w^{us_i}_{y}(y^{us}_i) - w^{us_{i+1}}_{y}(y^{us}_i) = 0, \tag{81}$$

$$w^i(y^i_t) = -\frac{v^{us}}{\sin(\beta_i)} + \frac{v^i}{\tan(\beta_i)}, \tag{82}$$

$$w^{us_i}(y^{us}_i) = -\frac{v^{us}}{\tan(\beta_i)} + \frac{v^i}{\sin(\beta_i)}, \tag{83}$$

$$-M^{us_i}_{yy,y}(y^{us}_i) + \lambda^{us}_i + M^{us_{i+1}}_{yy,y}(y^{us}_i) = 0, \tag{84}$$

$$-M^i_{yy,y}(y^i_t) + \lambda^t_i = 0. \tag{85}$$

The transverse continuity conditions along the lower nodal lines are

$$M^{ls_i}_{yy}(y^{ls}_i) - M^i_{yy}(y^i_b) + M^{ls_{i+1}}_{yy}(y^{us}_i) = 0, \tag{86}$$

$$w^{ls_i}_{,y}(y^{ls}_i) - w^{ls_{i+1}}_{,y}(y^{ls}_i) = 0, \qquad w^{i}_{,y}(y^i_b) + w^{ls_i}_{,y}(y^{ls}_i) = 0, \tag{87, 88}$$

$$w^{ls_i}_{y}(y^{ls}_i) - w^{ls_{i+1}}_{y}(y^{ls}_i) = 0, \tag{89}$$

$$w^i(y_b^i) = \frac{v^i}{\tan(\beta_i)} - \frac{v^{ls}}{\sin(\beta_i)}, \tag{90}$$

$$w^{ls}(y_i^{ls}) = \frac{v^i}{\sin(\beta_i)} - \frac{v^{ls}}{\tan(\beta_i)}, \tag{91}$$

$$-M_{yy,y}^{ls_i}(y_i^{ls}) + \lambda_i^{ls} + M_{yy,y}^{ls_{i+1}}(y_i^{ls}) = 0, \tag{92}$$

$$-M_{yy,y}^{i}(y_b^{j}) + \lambda_i^{b} = 0. \tag{93}$$

The longitudinal boundary conditions at the slabs ($j = us, ls$) read

$$N_{xx}^j = 0 \quad \text{or} \quad u_o^j = 0, \tag{94}$$

$$M_{xx}^j = 0 \quad \text{or} \quad v,_x^j = 0, \tag{95}$$

$$M_{xx,x}^j - \sum_{i=1}^{n_p} \lambda_i^{u,j} y_i^j = 0 \quad \text{or} \quad v^j = 0. \tag{96}$$

For each panel ($i = 1, \ldots, n_p$) they read

$$N_{xx}^i = 0 \quad \text{or} \quad u_o^i = 0, \tag{97}$$

$$M_{xx}^i = 0 \quad \text{or} \quad v,_x^i = 0, \tag{98}$$

$$M_{xx,x}^i + \lambda_i^{u,us} y_t^i + \lambda_i^{u,ls} y_b^i = 0 \quad \text{or} \quad v^i = 0. \tag{99}$$

The solution procedure of the free vibration problem in this case is similar to that of multi-girder bridges.

3. Numerical examples

Four numerical examples are presented and discussed. The results of each example are presented in terms of eigenfrequencies and eigenmodes. The results are compared with other results that have been determined by different mathematical models that appear in the literature, in order to examine the accuracy of such approximated models. Validation of the proposed model is achieved through comparison with three-dimensional finite element models. The numerical examples consist of: a simply supported bridge with a channel cross-section; a multi-girder bridge with cross beam; a simply supported and a continuous single-cell box bridge.

3.1. Example 1: simply supported bridge with a channel cross-section

Geometry and mechanical properties of the bridge, as well as sign convention of the proposed model appear in Fig. 5a. The bridge is simply supported at two rigid diaphragms. The main purpose of this case is to examine the effect of the transverse deformations on the eigenfrequencies of the bridge. In order to perform such investigation, the structure is solved by the proposed model and is compared with the classic beam theory, which takes into account torsional warping effects and neglects transverse deformations effects [8].

The first two eigenfrequencies and eigenmodes that are determined by the beam model appear in Fig. 5b. It is seen that the first eigenmode is the first vertical flexural mode with an eigenfrequency that equals: $f_1 = 21.6356$ Hz, and the second mode includes coupled horizontal flexure and torsional vibrations with eigenfrequency that equals: $f_2 = 23.7686$ Hz. The results of the proposed model appear in Fig. 5c, in terms of the eigenfrequencies and the normalized eigenmodes. The results reveal that the inclusion of the transverse deformations in the analysis

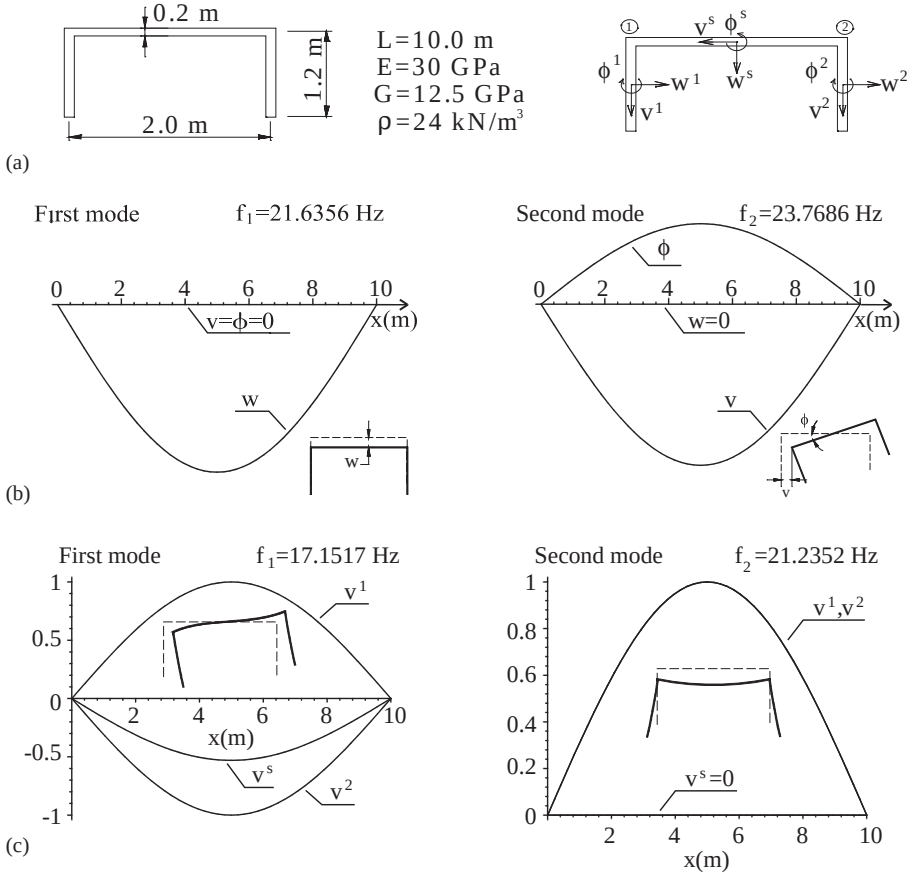

Fig. 5. A channel bridge: (a) geometry, mechanical properties and sign convention; (b) first and second eigenmodes determined by the beam model; (c) first and second eigenmodes and deformed section at midspan determined by the proposed model.

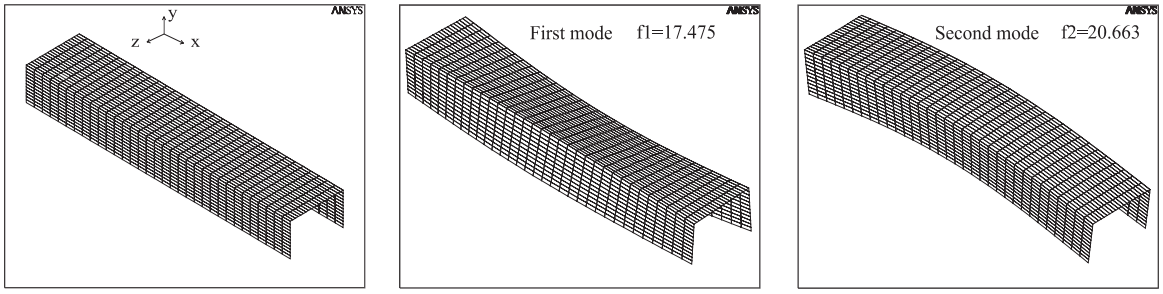

(a) (b) (c)

Fig. 6. Finite element model: (a) geometry and elements mesh; (b) first eigenmode (torsion); (c) second eigenmode (vertical flexure).

causes the first eigenmode to be a coupled flexural and torsional mode, as opposed to the beam model. It also changes the first eigenfrequency to: $f_1 = 17.1517$ Hz, which is about 30% less than that of the beam model. Hence, the transverse deformations drastically affect the eigenfrequency of the torsional eigenmode, and cause it to become the fundamental one. The influence of the transverse deformations on the vertical flexure eigenfrequency is much smaller (2%).

The results of the proposed model have been validated by comparison with the results of three-dimensional finite element model using ANSYS Version 5.7, with standard four-nodes shell elements. The FE model includes 8364 degrees-of-freedom, as shown in Fig. 6. The boundary conditions are modelled by imposing zero displacements in the y–z plane for all the nodes at the longitudinal edges of the bridge. The results of the FE model and those of the proposed model agree very well. Hence, using the classical beam theory for the modelling of even narrow bridges is erroneous.

3.2. Example 2: multi-girder bridge

The geometry of the bridge considered, is the one used by Wang et al. [12], and it appears in Fig. 7. The spatial weight of the concrete is $\rho = 25.7\ \mathrm{kN/m^3}$. The mechanical properties are defined based on some other papers by the authors. Wang et al. [12] have determined the eigenfrequencies using the grillage beam model (GRID). The sign convention of the current example is illustrated in Fig. 8a. The results of the proposed model appear in Fig. 8b, and are verified through comparison with three-dimensional FE modelling of the bridge. The results of the three models (proposed model, GRID, FE) are summarized in Table 1. It should be noted that all the torsional mode shapes are coupled with horizontal flexure of the bridge (see Fig. 8b).

The results of the proposed model and those of the FE model compare well and reveal that the torsional mode shape becomes the fundamental eigenmode of the bridge, while the results of the GRID model indicate that the torsional mode is related to the second eigenmode. This significant contradiction between the results is due to the fact that the GRID model uses equivalent longitudinal rigidity of the longitudinal beams, and does not consider their out-of-plane displacements. The results indicate that the eigenfrequency of the torsional eigenmode is reduced by about 12% when considering the transverse deformations of the structure. Furthermore, the second eigenmode of torsion that is indicated by the FE and the proposed models is not within the

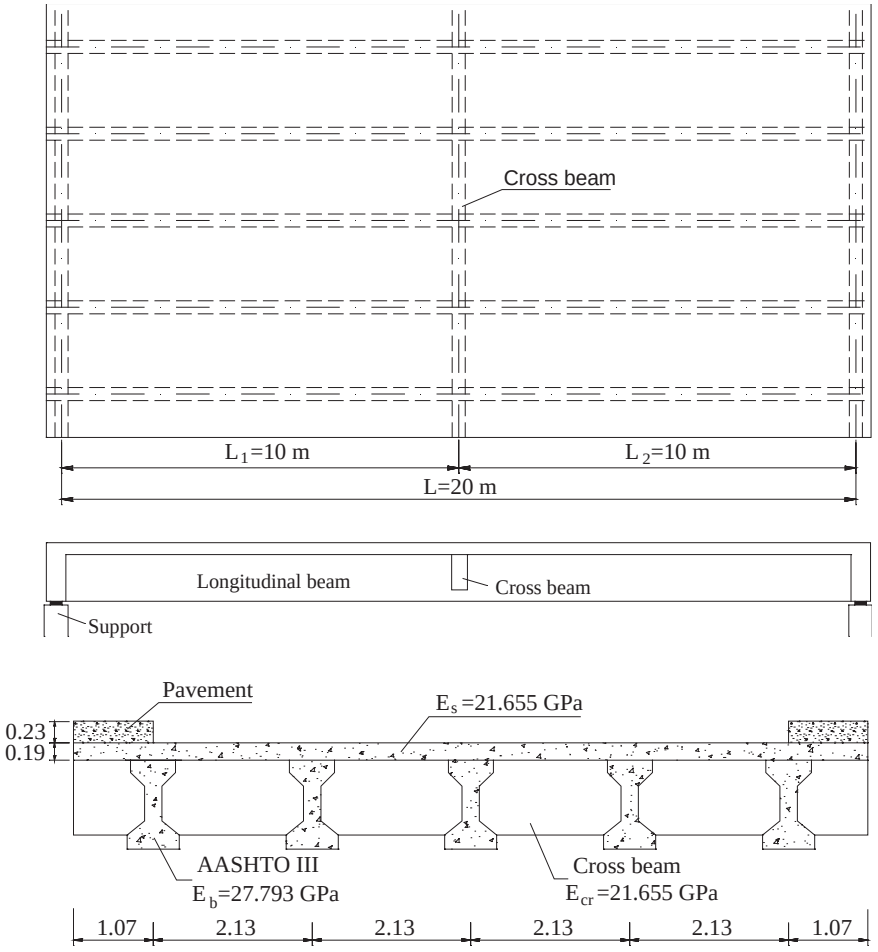

Fig. 7. Plane and typical cross-section of a multi-girder bridge case.

first four eigenmodes of the bridge in the GRID model. Notice that all eigenfrequencies that were determined by the GRID model are much higher than those of the proposed one, except for the eigenfrequency of the first vertical flexure. It means that the GRID model describes a much stiffer structure than the real one, and yields unreliable eigenfrequencies.

Please notice, that there is a very good correlation between the results of the FE model and the proposed one, except for the eigenfrequency of the transverse deformations mode shape. This is due to the fact that in the proposed model, it is assumed that the cross beam connection with the longitudinal beams is able to transfer only shear forces, while the FE and GRID models assume a rigid connection between the beams. It is important to indicate that in reality, this connection is not a rigid one, and the type of connection used in the proposed model is more appropriate and conservative.

The results of the bridge without a cross beam appear in Table 2, in order to validate that the difference between the FE results and the proposed model in the transverse deformation

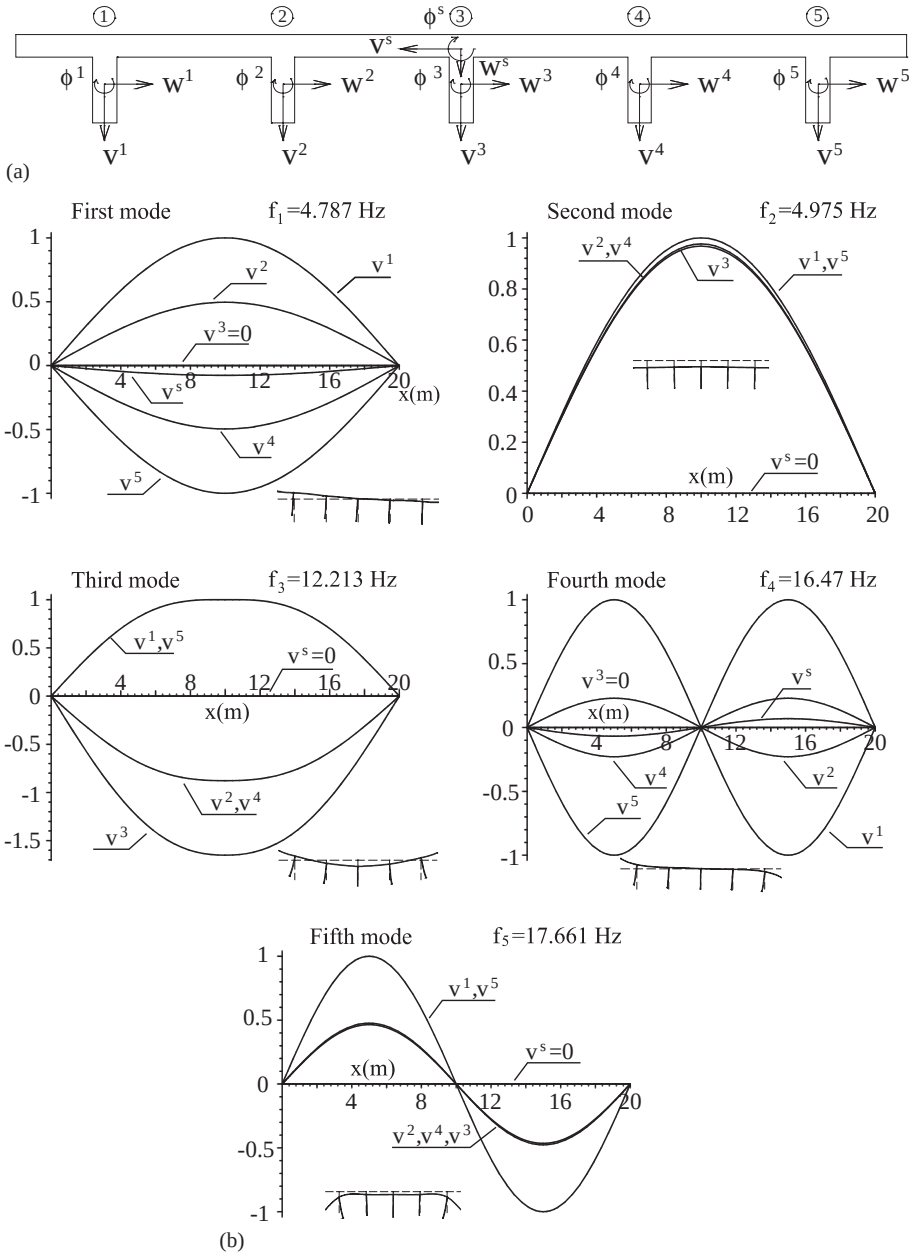

Fig. 8. A multi-girder bridge case: (a) sign convention; (b) eigenmodes and deformed section at critical location.

eigenmode is only due to different modelling of the connection of the cross beam. In this case, the results are compared with the equivalent orthotropic plate model [19]. Here, a very good agreement exists between the FE results and those of the proposed model for all eigenmodes. The results of the equivalent orthotropic plate model agree very well in the first two lower

Table 1
Eigenfrequencies and modes of a simply supported multi-girder bridge *with* cross beam

Mode shape	Eigenfrequency (Hz)		
	GRID [12]	Proposed model	Finite element
Vertical flexure	4.917	4.975	4.933
Torsion	5.455	4.787	4.86
Transverse deformation	16.167	12.213	15.395
Second torsion	–	16.47	16.333
Second vertical flexure	20.326	17.661	16.745

Table 2
Eigenfrequencies and modes of a simply supported multi-girder bridge *without* a cross beam

Mode no.	Mode shape	Eigenfrequency (Hz)		
		Proposed model	Finite element	Orthotropic plate
1	Torsion	4.907	4.962	5.147
2	Vertical flexure	5.088	4.989	5.015
3	Transverse deformation	7.365	7.663	6.455
4	Second transverse deformation	12.655	11.991	10.986
5	Second torsion	16.471	16.219	20.187
6	Second vertical flexure	17.661	16.242	20.060

eigenfrequencies, while large discrepancies exist in the higher ones. These discrepancies are due to the fact that the equivalent orthotropic plate model assumes uniform distribution of the rigidity and the mass through the width and the length of the bridge separately, which is far from the actual distribution.

3.3. Example 3: simply supported single-cell box bridge

The case discussed here consists of the geometry and mechanical properties of the bridge that appears in Ref. [15], and are described in Fig. 9a. Huang et al. have determined the eigenfrequencies and eigenmodes of the bridge by the finite element method according to the theory of thin-walled beams [16]. The warping torsion and distortion have been considered in their analysis. However, the distortion is considered in an approximated form, through a distortional angle of the cross-section. This modelling of the distortion ignores the transverse bending moments and the transverse inertial forces involved with the distortion of the cross-section. The results of the proposed model are presented in Fig. 9b and Table 3, and are verified through comparison with three-dimensional FE model using four-node shell elements.

The results of the proposed model and the thin-walled beam model agree well in the lower eigenfrequencies (first and second frequencies), and differ considerably in the higher eigenmodes. The results of the FE model correlate very well with those of the proposed model. This case

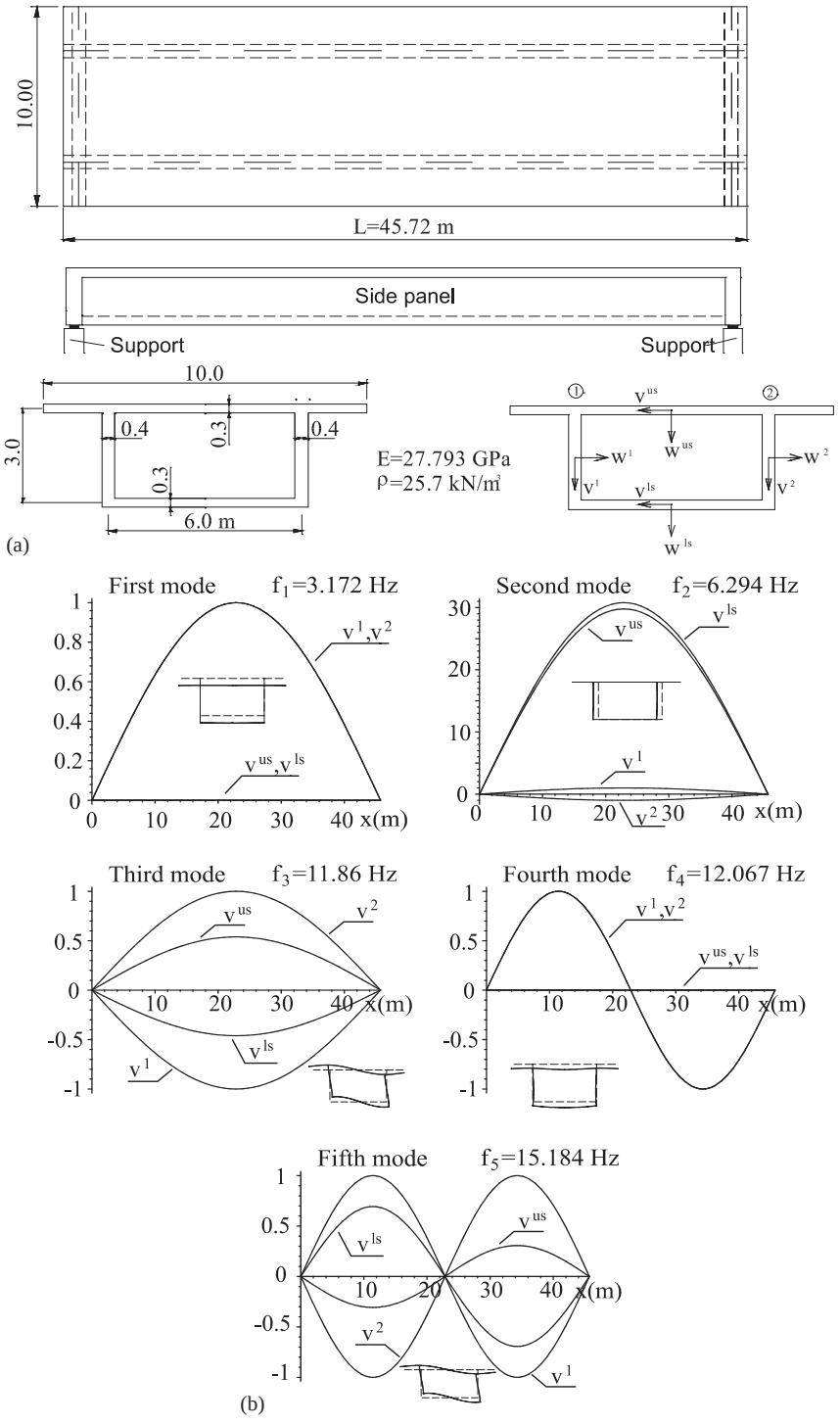

Fig. 9. A single-cell box bridge: (a) geometry, mechanical properties and sign convention; (b) eigenmodes and deformed section at critical location.

Table 3
Eigenfrequencies and modes of a simply supported single-cell box bridge

Mode shape	Eigenfrequency (Hz)		
	Thin-walled beam [15]	Proposed model	Finite element
Vertical flexure	3.22	3.172	3.203
Horizontal flexure	6.644	6.294	6.135
Second vertical flexure	12.983	12.067	11.265
Torsion	14.961	11.860	11.160
Second torsion	19.975	15.184	15.482

reveals that the thin-walled beam model proposed by Huang et al. [15], underestimates the high eigenfrequencies of single-cell box bridges, especially in the torsional eigenmodes. However, in bridges with a different layout, the torsional eigenmodes may become the lower ones, which may drastically affect the dynamic behaviour of the bridge.

3.4. Example 4: continuous single-cell box bridge

This case is presented in order to describe the capability of the proposed model. The bridge scheme appears in Fig. 10a. It consists of the same cross-section, as well as the same mechanical properties of the previous case (see Fig. 9a). The results of the proposed model appear in Fig. 10b. The results of the proposed model compared with those of the FE model appear in Table 4, and reveal good comparison.

4. Summary and conclusions

The free vibration behaviour of multi-girder and multi-cell box bridges, including transverse deformations effects has been presented. The governing equations of motion and the boundary and continuity conditions are derived using the variational principle of virtual work following Hamilton's principle. The model is valid for any combination of boundary and continuity conditions, and is applicable for any multi-girder bridges with cross beams and for multi-cell box bridges. Lagrange multipliers are included in order to impose identical deformations of the various constituents of the structure (slab and beams) through the nodal lines, and to fulfill other compatibility requirements. Here, warping and distortion of the bridge cross-section are considered accurately. Closed-form solution for the governing equations of motion has been achieved, and the eigenfrequencies are determined using the Newton–Raphson method.

Numerical examples have been presented to validate the proposed model, and to examine the accuracy of other approximate models that appear in the literature, such as: the beam model; the GRID model; the equivalent orthotropic plate model; and the thin-walled beam model. The conclusions that have been drawn in regard to these methods appear in Section 3 (numerical examples). Validation of the proposed model has been achieved through comparison with three-dimensional finite element models using four-node standard shell elements, which in all cases indicates a very good correlation.

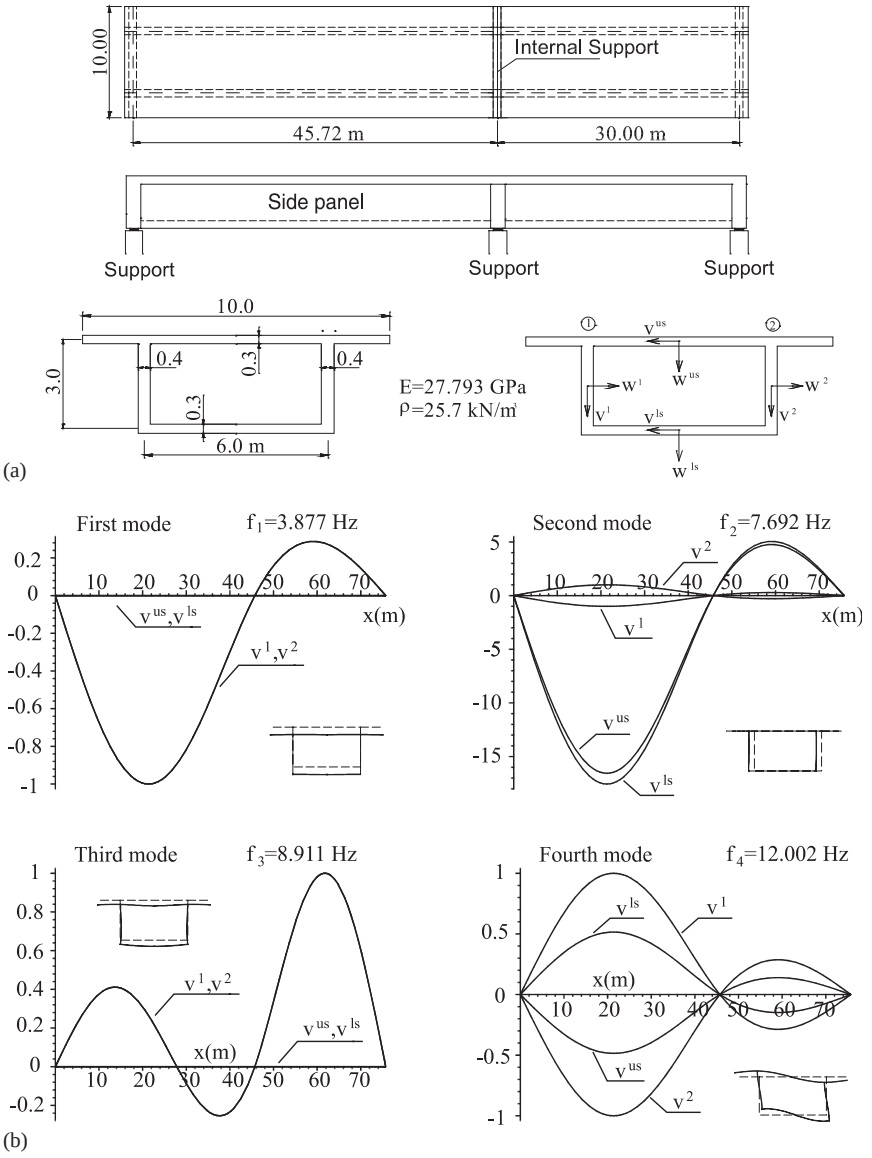

Fig. 10. A continuous single-cell box bridge: (a) plane view; (b) eigenmodes and deformed section at critical location.

Finally, it should be noted that the conventional dynamic design of bridges assumes that the vertical flexural eigenmode is the fundamental one, which differ from reality and affects the safety of the structure. The results of the proposed model reveal that the transverse deformations significantly reduce the eigenfrequencies of multi-girder and multi-cell box bridges, and in some cases it caused the torsional eigenmodes to become the fundamental ones. Hence, in order to achieve reliable bridges, it is recommended to consider the transverse deformations in the static and dynamic analysis of bridges.

Table 4
Eigenfrequencies and modes of a continuous single-cell box bridge

Mode no.	Mode shape	Eigenfrequency (Hz)	
		Proposed model	Finite element
1	Vertical flexure	3.877	3.840
2	Horizontal flexure	7.692	7.264
3	Vertical flexure	8.911	8.326
4	Torsion	12.002	11.325

References

[1] M. Wieland, M.J. Inbanathan, Bridge vibrations due to vehicle moving over rough surface, *American Society of Civil Engineers Journal of Structural Engineering* 113 (9) (1987) 1994–2007.
[2] P.K. Chatterjee, T.K. Datta, C.S. Surana, Vibration of continuous bridges under moving vehicles, *Journal of Sound and Vibration* 169 (5) (1994) 619–632.
[3] S. Shore, S. Chaudhuri, Free vibration of horizontally curved beams, *American Society of Civil Engineers Journal of the Structural Division* 98 (3) (1972) 793–796.
[4] P. Heins, A. Sahin, Natural frequency of curved box girder bridges, *American Society of Civil Engineers Journal of the Structural Division* 105 (12) (1979) 2591–2599.
[5] M. Kawatani, Y. Kobayashi, K. Takamori, Nonstationary random analysis with coupling vibration of bending and torsion of simple girder bridges under moving vehicles, *Structural Engineering/Earthquake Engineering* 15 (1) (1998) 107–114.
[6] V.Z. Vlasov, *Thin-Walled Elastic Beams*, National Science Foundation, Washington, 1961.
[7] R. Dabrowski, *Curved Thin-Walled Girders, Theory and Analysis*, Springer, Berlin, 1968 (Translation from German).
[8] S. Timoshenko, D.H. Young, W.J.R. Weaver, *Vibration Problems in Engineering*, 4th Edition, Wiley, New York, 1974.
[9] S.G. Hutton, Y.K. Cheung, Dynamic response of single span highway bridges, *Earthquake Engineering and Structural Dynamics* 7 (1979) 543–553.
[10] N. Taysi, M. Ozakca, Free vibration analysis and shape optimization of box-girder bridges in straight and curved platform, *Engineering Structures* 24 (5) (2002) 625–637.
[11] K. Gupta, Dynamic loading of highway bridges, *Journal of the Engineering Mechanics Division* 106 (2) (1980) 377–394.
[12] T. Wang, D. Huang, M. Shahawy, Dynamic response of multigirder bridges, *American Society of Civil Engineers Journal of Structural Engineering* 118 (8) (1993) 2222–2238.
[13] D.P. Thambiratnam, G.H. Brameld, Free vibration analysis of bridges, *Engineering Structures* 17 (10) (1995) 705–713.
[14] D.R. Schelling, N.H. Galdos, M.A. Sahin, Evaluation of impact factors for horizontally curved steel box bridges, *American Society of Civil Engineers Journal of Structural Engineering* 118 (11) (1992) 3203–3221.
[15] D. Huang, T. Wang, M. Shahawy, Vibration of thin-walled box-girder bridges excited by vehicles, *American Society of Civil Engineers Journal of Structural Engineering* 121 (9) (1995) 1330–1336.
[16] G.H. Li, *Analysis of Box Girder and Truss Bridges*, China Academic Publishers, Springer, Heidelberg, 1987.
[17] M.S. Cheung, A. Megnounit, Parametric study of design variations on the vibration modes of box girder bridges, *Canadian Journal of Civil Engineering* 18 (5) (1991) 789–798.
[18] K.M. Sennah, J.B. Kennedy, Dynamic characteristics of simply supported curved composite multi-cell bridges, *Canadian Journal of Civil Engineering* 24 (4) (1997) 621–636.
[19] L.A. Clark, *Concrete Bridge Design to BS 5400*, Construction Press, London, New York, 1983.